Validation of ASTER/TIR Standard Atmospheric Correction Using Water Surfaces

Hideyuki Tonooka, *Member, IEEE,* and Frank D. Palluconi

***Abstract*—The standard atmospheric correction algorithm for the five thermal infrared (TIR) bands of the Advanced Spaceborne Thermal Emission and Reflection Radiometer (ASTER) is based on radiative transfer calculation using the MODTRAN code. Atmospheric profiles input to MODTRAN are extracted from either the Global Data Assimilation System (GDAS) product or the Naval Research Laboratory (NRL) climatology model. The present study provides validation results of this algorithm. First, *in situ* lake surface temperatures measured in 13 vicarious calibration (VC) experiments were compared with surface temperatures retrieved from ASTER data. As the results, the mean bias was 0.8 and 1.8 K for GDAS and NRL, respectively. The NRL model performed worse than GDAS for four experiments at Salton Sea, CA, probably because the model was not suitable for this site, which has typically higher surface temperature and humidity than other VC sites. Next, the algorithm was validated based on the max-min difference (MMD) of water surface emissivity retrieved from each of 163 scenes acquired globally. As a result, the algorithm error increased quadratically with the precipitable water vapor (PWV) content of the atmosphere, and the expected MMD error was 0.049 and 0.067 for GDAS and NRL, respectively, with a PWV of 3 cm, where 0.05 on MMD is roughly corresponding to -0.8 or $+2.3$ K on the retrieved surface temperature error. The algorithm performance degraded markedly when the surface temperature exceeded about 25 °C, particularly for NRL. Consequently, GDAS performs better than NRL as expected, while both will perform less well for humid conditions.**

***Index Terms*—Emissivity, MODTRAN, National Centers for Environmental Prediction (NCEP)/Global Data Assimilation System (GDAS), Naval Research Laboratory (NRL) climatology model, precipitable water vapor (PWV), radiative transfer, temperature, vicarious calibration.**

I. Introduction

THE radiation reflected at or emitted from Earth surfaces will be modified by atmospheric scattering, attenuation, and emission, before reaching a satellite sensor. Atmospheric correction is, therefore, necessary for the retrieval of Earth surface parameters. In the Advanced Spaceborne Thermal Emission and Reflectance radiometer (ASTER) project [1], the surface radiance, reflectance, emissivity, and temperature are retrieved by standard algorithms on demand to be delivered to a user. This paper provides an assessment of standard atmospheric correction for the thermal infrared (TIR) bands of the ASTER instrument. Several studies have verified atmospheric correction for ASTER/TIR using actual ASTER data or alternative airborne sensor data [2], [3], but they were conducted using only a few scenes. This paper focuses on validation of the standard atmospheric correction under various conditions in global. The validation involves two approaches, a traditional *in situ* temperature-based approach, and an original emissivity-based approach [4]. These approaches are applied to water surfaces such as lakes and seas.

Manuscript received October 29, 2004; revised July 23, 2005.

H. Tonooka is with the Ibaraki University, Ibaraki 316-8511, Japan (e-mail: tonooka@mx.ibaraki.ac.jp).

F. D. Palluconi is with the Jet Propulsion Laboratory, Pasadena, CA 91109 USA.

Digital Object Identifier 10.1109/TGRS.2005.857883

TABLE I
SUMMARY CHARACTERISTICS OF THE ASTER/TIR SUBSYSTEM

Spatial resolution	90 m
Swath width	60 km
Signal quantization levels	12 bits
NEΔT	$\leq$ 0.3 K
Absolute temperature accuracy (design values)	$\leq$ 3 K (200–240 K)
	$\leq$ 2 K (240–270 K)
	$\leq$ 1 K (270–340 K)
	$\leq$ 2 K (340–370 K)
Spectral band passes	Band 10: 8.125–8.475 μm
	Band 11: 8.475–8.825 μm
	Band 12: 8.925–9.275 μm
	Band 13: 10.25–10.95 μm
	Band 14: 10.95–11.65 μm

II. ASTER

The ASTER instrument is a high spatial resolution multispectral imager on the Terra spacecraft—the first platform of the National Aeronautics and Space Administration's Earth Observing System—launched in December 1999. ASTER consists of three subsystems, each covering different parts of the electromagnetic spectrum: the visible and near infrared (VNIR), the short-wave infrared (SWIR), and the thermal infrared subsystems. The ASTER/TIR subsystem has five spectral bands (bands 10–14) with a spatial resolution of 90 m. These bands allow the retrieval of both surface temperature and surface spectral emissivity, which can be used in a wide variety of studies such as environmental monitoring, geological mapping, and hazard prediction. Table I shows summary characteristics of the ASTER/TIR subsystem.

The ASTER/TIR subsystem obtains images by mechanical scanning with ten mercury–cadmium–telluride photoconductive detectors which are aligned along the track for each band (50 detectors in total) and cooled to 80 K using a mechanical split Stirling cycle cooler [5]. The digital number (DN) obtained by each detector is radiometrically calibrated using a single

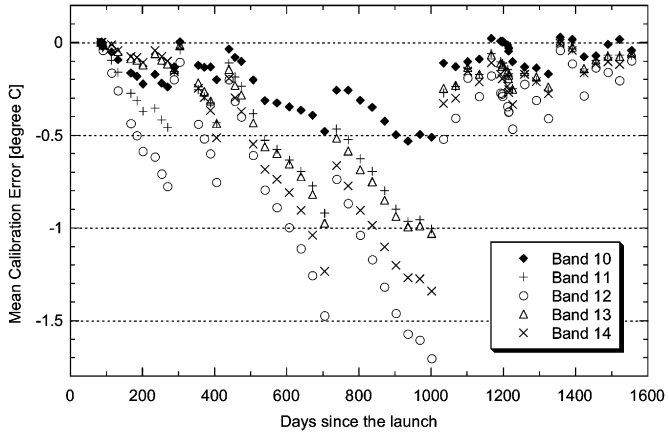

Fig. 1. Predicted calibration error of the original ASTER/TIR radiance at 300 K (not recalibrated), averaged over detectors for each band, as a function of the days since the launch (December 18, 1999).

onboard blackbody. The blackbody is set to 270 K for the offset adjustment before every Earth observation. The gain coefficient is periodically measured by long-term calibration (LTC) in which the blackbody is observed at 270, 300, 320, and 340 K. Not every LTC result is applied to the level-1 products.

Recent studies have demonstrated that the level-1 products contain a calibration error caused by delays in updating the gain coefficients in the level-1 software [6], [7]. A user-based recalibration method has been developed to correct for these delay-induced errors [6], and the necessary coefficients to apply this correction to a given scene can be obtained through Internet.[1] Fig. 1 shows the predicted calibration error of the original radiance at 300 K (not recalibrated), averaged over detectors for each band, as a function of the days since the launch (December 18, 1999). The error on the recalibrated radiance would be within almost ± 0.2 K in temperature.

More detailed descriptions on ASTER/TIR radiometric calibration can be found in [7].

III. Theoretical Basis

In the TIR region (8–14 μm in wavelength), reflected solar radiation is a much smaller component of the observed signal than the Earth emitted radiation. In addition, the atmospheric downward radiance at ground level is smaller than the surface emitted radiance, and the surface reflectance in this spectral region is generally small. Thus, the assumption that the surface is a Lambertian surface will not produce a large error [8], and will be reasonable particularly for ASTER/TIR which has the swath width of 60 km and the maximum pointing angle of $\pm 8.55^\circ$. Hence, the at-sensor radiance under a clear sky condition can be expressed by

$$I_\lambda(\theta) = \tau_\lambda(\theta)\left[\epsilon_\lambda B_\lambda(T_s) + \frac{(1-\epsilon_\lambda)F_\lambda^\downarrow}{\pi}\right] + I_\lambda^\uparrow(\theta) \qquad (1)$$

where

λ	wavelength;
θ	view angle;
ϵ_λ	surface emissivity;
T_s	surface kinetic temperature;
$B_\lambda(T_s)$	Planck function;
$\tau_\lambda(\theta)$	atmospheric transmittance;
$I_\lambda^\uparrow(\theta)$	path radiance;
$F_\lambda^\downarrow$	downward atmospheric irradiance at ground level.

In this paper, $\tau_\lambda(\theta)$, $I_\lambda^\uparrow(\theta)$, and $F_\lambda^\downarrow$ are generically called atmospheric effect parameters.

In practical cases, (1) is approximately rewritten [9] as

$$I_i(\theta) = \tau_i(\theta)\left[\epsilon_i B_i(T_s) + \frac{(1-\epsilon_i)F_i^\downarrow}{\pi}\right] + I_i^\uparrow(\theta) \qquad (2)$$

where each variable x_i with the subscript i is the weighted mean over λ with the normalized response function $\phi_{i,\lambda}$ of band i

$$x_i = \int_0^\infty \phi_{i,\lambda} x_\lambda d\lambda. \qquad (3)$$

The atmospheric effect parameters ($\tau_i(\theta)$, $I_i^\uparrow(\theta)$, and $F_i^\downarrow$) can be calculated by a radiative transfer code such as MODTRAN [10], combined with atmospheric profiles and elevation data. Thus, the at-surface radiance $I_{s,i}$ is derived from the at-sensor radiance by

$$I_{s,i} = \frac{I_i(\theta) - I_i^\uparrow(\theta)}{\tau_i(\theta)} \qquad (4)$$

where $I_{s,i}$ is expressed by

$$I_{s,i} = \epsilon_i B_i(T_s) + \frac{(1-\epsilon_i)F_i^\downarrow}{\pi}. \qquad (5)$$

Atmospheric correction based on this approach has been applied in various studies [2], [3], [11]–[15].

Even if $I_{s,i}$ is derived, ϵ_i and T_s cannot easily be obtained, because the number of unknown parameters (ϵ_i and T_s) is always one more than the number of simultaneous equations available for solution: e.g., ASTER/TIR has six unknown parameters (five emissivities for the five bands plus one temperature) with only five simultaneous equations available for the five bands at each pixel. Thus, a number of temperature/emissivity separation methods have been proposed for solution of this problem. A typical solution is to add an empirical emissivity equation based on the known properties of terrestrial materials to the simultaneous equation set. For example, the normalized emissivity method (NEM) [16] separates temperature and emissivity by adding the equation of "$\epsilon_{\max} = \text{const.}$" assuming that the maximum emissivity over bands is constant over the image.

IV. Standard Atmospheric Correction for ASTER/TIR

A. Overview

In the TIR spectral region, differential absorption algorithms such as the split-window method are well known as practical ways of atmospheric correction [17]–[19]. These algorithms can reduce atmospheric effects by combining brightness temperatures measured in two or more channels/angles, and have operationally been used for retrieval of sea surface temperature (SST) from Advanced Very High Resolution Radiometer data [20] since the 1980s. But these algorithms cannot easily be applied for land observations, since uncertainty in emissivity will

[1] http://www.science.aster.ersdac.or.jp/RECAL/

often introduce a significant error [21]. Although some improvements have been proposed for land observations [22]–[26], they basically need some information on surface emissivity for each pixel. In the case of ASTER/TIR, not only the surface temperature but also the surface spectral emissivity should be provided as standard products, and also all the TIR bands are located in the clearest part of the atmospheric window in the TIR region. Thus, not the different absorption algorithms but the radiative transfer-based algorithm [(4) and (5)] has been used for ASTER/TIR atmospheric correction [27].

The standard atmospheric correction for ASTER/TIR is applied to a level-1B scene (registered scaled radiance at the sensor) [1] on demand by a user through web sites,[2] and the product is then delivered to the user.

B. Procedure of Standard Atmospheric Correction

The standard atmospheric correction uses the atmospheric effect parameters ($\tau_i(\theta)$, $I_i^{\uparrow}(\theta)$, and $I_i^{\downarrow}$) calculated by the MODTRAN code (the implemented version is 3.5), combined with atmospheric profiles and elevation data. Although this correction is on a pixel-by-pixel basis, the following interpolation is used for reduction of processing time. First, the input data to MODTRAN are interpolated to a uniform grid across an ASTER image (60×60 km). Next, the atmospheric effect parameters for each grid point are calculated for several elevations representative of the surrounding terrain, and then those for each pixel are determined by spatial interpolation from the surrounding grid points as a function of latitude, longitude, and elevation. This procedure will not produce any significant additional error, because all the primary input data to MODTRAN, including surface elevation, are available only at lower resolution than ASTER/TIR's 90-m pixel (the horizontal resolution is 1° in atmospheric profiles, and 1 km in elevation, as mentioned below).

C. Primary Atmospheric Profiles Input to MODTRAN

The atmospheric profile data input to the code should match each image in space and time. In particular, the match of humidity and air-temperature profiles is important for better accuracy. Currently, the following atmospheric sources have been used in ASTER/TIR atmospheric correction. The source that is used is determined on demand by a user at the time an atmospherically corrected product is ordered through the web sites.[2]

1) GDAS Product: The Global Assimilation System (GDAS) [28] operated by National Centers for Environmental Prediction (NCEP) is a typical four-dimensional real-time analysis system for providing a first guess to other numerical forecast systems. The GDAS assimilates various meteorological data measured by radiosondes, ships, planes, satellites, ground stations, etc., and forecasts the next atmospheric situation in global. The system outputs various atmospheric parameters, such as temperature, humidity, geopotential height, and wind speed, for each three-dimensional grid-point at 6-h intervals. In the standard atmospheric correction, air temperature, humidity, and geopotential height are extracted from GDAS products which have 1° horizontal spacing and 28 vertical layers up to 2.7 hPa, and spatially temporally interpolated profiles are then input to MODTRAN.

2) NRL Climatology: The Naval Research Laboratory (NRL) climatology [29] is a model generated from observational datasets and one-dimensional and two-dimensional chemical–dynamical model result. The model includes zonally averaged atmospheric profiles for altitudes up to 120 km for 27 species (pressure, temperature, total density, H_2O mixing ratio, etc.) for each month at 10° spacing in latitude. In the standard atmospheric correction, pressure, air temperature, and H_2O mixing ratio at each height in the observation month of each ASTER image are interpolated in latitude, and input to MODTRAN. This profile set, which is based on climatology, is to be used only when no other profile information is available and an atmospherically corrected ASTER product is still needed. Because it cannot be specific to the time and location of ASTER images, it is expected to be the least accurate source for atmospherically correcting ASTER TIR data.

In the original plan [27], the Moderate Resolution Imaging Spectroradiometer (MODIS) atmospheric profile product (MOD07) [30] was the prime option, while GDAS was a backup option, but GDAS and NRL have been used as a primary and backup options, respectively, until now, because validation of the product MOD07 has taken some time. Although the MOD07 option has not yet been implemented at present, it may be available in the future.

D. Other Atmospheric Data Input to MODTRAN

The other atmospheric profiles not described above are basically derived from the U.S. standard 1976 model included in MODTRAN except for O_3, CH_4, CO, and N_2O. Although these four species are not significant for ASTER/TIR bands, the O_3 profile is modified with the total ozone product of the Total Ozone Mapping Spectrometer (TOMS) [31], and the profiles of CH_4, CO, and N_2O are extracted from the NRL model. Since aerosols are often not significant, the Rural-Visibility $= 23$ km model with seasonal modification, included in MODTRAN, is used for all ASTER images.

E. Elevation

The surface elevation of each pixel is given by interpolation from Global 30 Arc Second Elevation Data Set (GTOPO30) [32] as a function of latitude and longitude. Since GTOPO30 is based on data derived from eight sources of elevation information, the absolute vertical accuracy of GTOPO30 varies by location according to the source data [32]. For example, the root mean square (rms) error is 18 m in digital terrain elevation data (DTED) and the U.S. geological survey digital elevation model (DEM), and 97 m in the digital chart of the world [32]. In the standard atmospheric correction, an elevation error is probably larger than these errors because of interpolation from 30-arcsec grid point to 90-m grid point. The maximum atmospheric correction error caused by an elevation error is about 0.3 K per 100 m of elevation [27]. If the ASTER DEM product [1] is utilized in the future, such error may be reduced.

[2]Namely, the Earth Remote Sensing Data Analysis Center, the ASTER Ground Data System: http://imsweb.aster.ersdac.or.jp/ and the Land Processes Distributed Active Archive Center, Earth Observing System data gateway: http://edcimswww.cr.usgs.gov/pub/imswelcome/.

V. Validation Based on *In Situ* Measured Temperature

A. Overview

If some of surface parameters within a corrected image are known, atmospheric correction algorithms can be verified by comparison of the known value and the retrieved value. If surface temperature or radiance is used for this purpose, *in situ* measurements at the same location and time as each ASTER image are basically necessary, since these parameters are variable in time and space. In this section, the standard atmospheric correction is evaluated using *in situ* lake surface temperatures measured in vicarious calibration activities for ASTER/TIR.

B. Vicarious Calibration Activities for ASTER/TIR

Vicarious calibration (VC) is an inflight or on-orbit technique in which calibrated ground-based or airborne radiometers deployed on or above a spectrally and spatially homogeneous target take simultaneous measurements during periods of aircraft or satellite instrument overpasses [33]. Since the launch of Terra, the ASTER science team has conducted a number of VC experiments for all bands of the ASTER instrument [34]. For the five TIR bands, we have conducted VC experiments on lakes and playas (dry lakes). More detailed descriptions on VC for ASTER/TIR can be found in [7].

C. In Situ Measurements of Lake Surface Kinetic Temperature

Water is a good target for VC because it is uniform in composition, has a high and known emissivity, and often exhibits low surface temperature variation (≤ 1 °C) over large areas [35]. To provide an estimate of bulk water temperature we used temperature measuring buoys (five to nine buoys) dispersed over an area covering 3×3 ASTER pixels in area (270×270 m). These buoys can measure and record the bulk water temperature at about 2–3 cm beneath the water surface, but the bulk water temperature is not the radiating, kinetic, or skin temperature of the water surface which is sensed by ASTER. To determine the difference between the bulk water temperature and the water surface radiating temperature, we simultaneously measured the brightness temperature of the water surface with a well-calibrated radiometer near the location of one of the buoys. The surface kinetic temperature was then derived from the brightness temperature by correcting for the water emissivity and the downward atmospheric irradiance. More detailed descriptions on this topic can be found in [7].

Table II is a list of 13 VC experiments evaluated in this paper, giving the date, the site name, the lake surface kinetic temperature measured on site, and the precipitable water vapor (PWV) obtained from GDAS profile, for each experiment. These experiments are part of VC experiments conducted for ASTER/TIR on Lake Tahoe, CA, Salton Sea, CA, and Lake Kasumigaura, Japan, under clear sky conditions.

TABLE II
List of 13 VC Experiments Evaluated in This Paper, Giving the Date, the Site Name, the Lake Surface Kinetic Temperature Measured on Site, and the PWV Obtained From GDAS Profile, for Each Experiment

Date	Site	Surface kinetic temp. [°C]	PWV [cm]
2000/3/12	Lake Tahoe	5.8	0.57
2000/5/16	Kasumigaura	21.4	1.65
2000/6/4	Salton Sea	27.6	1.64
2000/11/7	Lake Tahoe	10.8	0.64
2001/3/16	Kasumigaura	8.9	0.39
2001/6/7	Salton Sea	28.6	1.95
2002/1/17	Salton Sea	14.2	0.54
2002/2/15	Kasumigaura	6.2	0.43
2002/3/19	Kasumigaura	12.4	0.59
2002/12/3	Salton Sea	18.5	1.61
2003/6/29	Salton Sea	29.5	1.64
2004/1/20	Kasumigaura	3.8	0.44
2004/2/5	Kasumigaura	4.9	0.40

D. Retrieval of Lake Surface Kinetic Temperature From ASTER Data

As mentioned in Section II, ASTER data contain a calibration error caused by delays in updating the gain coefficients in the level-1 software [6], [7]. This error depends on the scene observation date, the temperature, the detector, and the band, and can impact retrieval of surface parameters. In this paper, all the ASTER data used were first recalibrated by the recalibration method [6], although the radiance change in the 13 scenes used was not very large (0.02–0.05 $\mathrm{W/m^2/sr/\mu m}$ in radiance, or 0.1 °C to 0.3 °C in temperature).

The standard atmospheric correction was then applied to the recalibrated data. Atmospheric profiles for each scene were extracted from each of GDAS and NRL in the same ways described in Section IV-C. The atmospheric effect parameters ($\tau_i(\theta)$, $I_i^{\uparrow}(\theta)$, and $I_i^{\downarrow}$) were calculated by MODTRAN 3.7, combined with the atmospheric profiles from each of GDAS and NRL and the elevation of each site, and then integrated over wavelength with the spectral response function of each band. The surface radiance in each band was derived from (4) using the observed recalibrated radiance, the transmittance, and the path radiance, for each of GDAS and NRL.

The lake surface kinetic temperature and emissivity were then derived from the surface radiance and the downward atmospheric irradiance using the NEM with the maximum emissivity of 0.99 (this value was determined from water emissivity in the spectral library [36]).

E. Results

Fig. 2 displays the temperature difference (the difference of the retrieved temperature to the *in situ* temperature) for GDAS and NRL as a function of the *in situ* temperature, and Fig. 3 shows the temperature difference for each experiment. As shown, almost all cases demonstrate a positive difference. This would be caused by overcorrection at the maximum emissivity band which was band 13 or 14 except for Salton Sea on June 4, 2000 (band 10). GDAS demonstrates the temperature difference within 1 °C except for Salton Sea on June 4, 2000. The NRL climatology model demonstrates much worse results than GDAS for the four experiments at Salton Sea probably because the model is not suitable for the Salton Sea area which has typically higher surface temperature and humidity than other VC sites, but the NRL model exhibits similar performance to

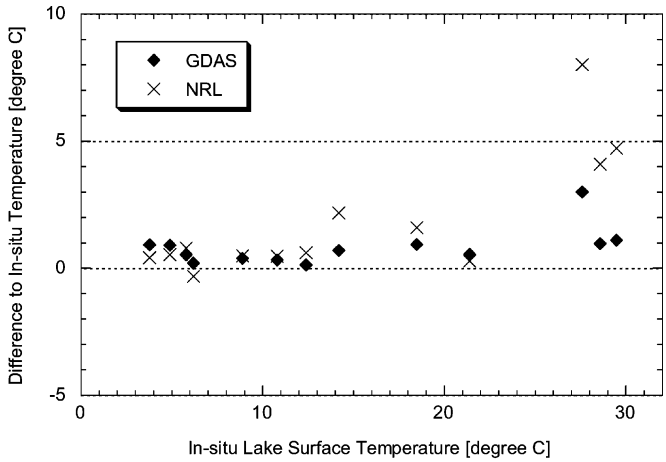

Fig. 2. Difference of the lake surface kinetic temperature (the retrieved temperature minus the *in situ* temperature) for GDAS and NRL as a function of the *in situ* temperature.

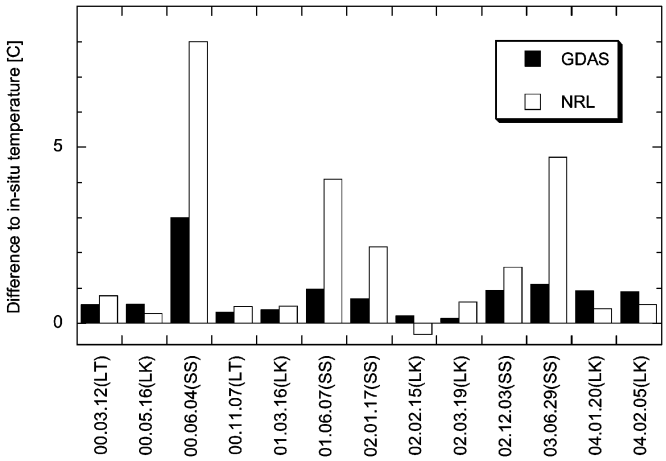

Fig. 3. Histogram of the difference of the lake surface kinetic temperature (the retrieved temperature minus the *in situ* temperature) for GDAS and NRL (LT: Lake Tahoe, LK: Lake Kasumigaura, SS: Salton Sea). The temperature difference is within 1 °C for GDAS except for Salton Sea on June 24, 000, while NRL gives large temperature differences for most of the Salton Sea experiments.

GDAS for the other experiments. The mean bias was 0.8 °C and 1.8 °C for GDAS and NRL, respectively. If the four Salton Sea experiments were excluded, they decreased to 0.5 °C and 0.4 °C, respectively. However, the mean bias obtained here will be smaller than the expected error in global conditions, because VC experiments have been usually conducted under lower humidy conditions by design.

VI. Validation Based on Water Surface Emissivity Retrieved

A. Overview

Surface temperature or radiance are not always easy to use for global-based validation of atmospheric correction algorithms, because *in situ* measurements are necessary. Surface emissivity is also variable due to various factors such as soil water content, condensation, snow/vegetation cover, and rock type [37], but the emissivity of water surfaces is almost invariable, although it will be slightly affected by wave (wind) or bubble [37], [38]. In addition, since surface spectral emissivity is an important productin the ASTER Project, atmospheric correction should work for surface spectral emissivity as well as for surface temperature. Consequently, matching the expected water surface spectral emissivity is an appropriate approach for global-based validation of atmospheric correction algorithms for ASTER/TIR.

In this section, we validate the standard atmospheric correction based on the max-min difference (MMD) of water surface emissivity retrieved [4]. Surface temperature and emissivity were separated from atmospherically corrected radiance by the NEM in which the maximum emissivity assumed to be constant was set to a value derived from a spectral library [36]. Since all targets in this validation study are water bodies and the maximum emissivity of water is known, the NEM will not produce a significant error. Thus, we can use the MMD of water surface emissivity retrieved as an index of atmospheric correction performance. Although the MMD of the retrieved surface brightness temperature may be also available, we did not use this approach, because the brightness temperature's MMD is a function of the temperature itself while the emissivity's MMD is free from the temperature.

B. Preliminary Simulation Study

The MMD of the retrieved water emissivity will allow validation of atmospheric correction under global conditions, but it is a "relative" approach. That is, MMD will indicate a spectral-contrast change caused by an atmospheric correction error, but have almost no information on a bias error in all bands, because bias effects will be subtracted through temperature/emissivity separation. As a preliminary study, we therefore investigated the relationship between the MMD of the retrieved emissivity (relative index) and the error on the retrieved temperature (absolute index) using a simulation model.

Atmospheric profiles of geopotential height, air temperature, and humidity were derived from monthly mean products (2.5° grid-point spacing) for January and July from 1979 to 1995 in the NCEP Climate Data Assimilation System (CDAS) reanalysis project.[3] For each month, 482 grid-points were selected uniformly from grid-points on global lands in the products, and then nine profile sets were produced for each of 964 profile sets (482 points × 2 months) by a combination of shifting in the temperature profile (-2, $+0$, $+2$ K) and scaling in the humidity profile ($\times 0.8$, $\times 1.0$, $\times 1.2$), thus generating 8676 profile sets ($= 964$ sets $\times$ 9 modifications). For each profile set, two surface temperatures were given by the surface air temperature (T_a) of each set and $T_a + 5$. Thus, the top-of-the atmosphere (TOA) radiances at ASTER/TIR bands were calculated by MODTRAN 3.7 for each of 17 352 conditions ($= 8676$ profile sets $\times$ 2 surface temperatures) according to (2), where the surface emissivity was given from water emissivity in the library [36], the surface elevation for each grid-point was given from the CDAS product, and the satellite altitude and the view angle were assumed to be 705 km and the nadir. Next, all the TOA radiances were atmospherically corrected using the standard algorithm but the original profiles ($+0$ K in temperature and $\times 1.0$ in humidity) of each profile set were used instead of that profile set to simulate an atmospheric correction error. Finally, the NEM ($\epsilon_{\max} = 0.99$) was

[3]http://www.cpc.ncep.noaa.gov/products/wesley/reanalysis.html

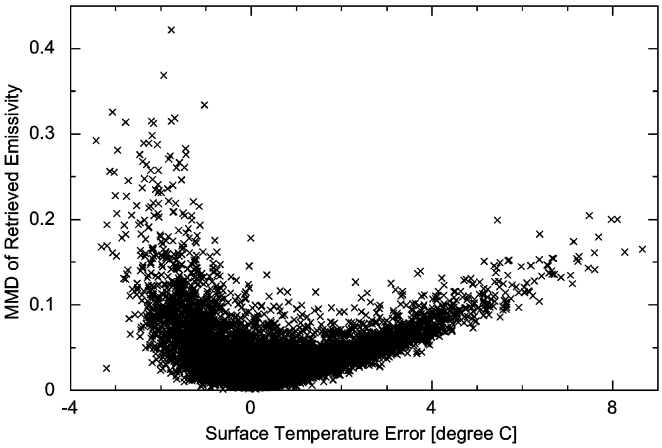

Fig. 4. Relationship between the MMD of the retrieved emissivity and the error on the retrieved surface temperature.

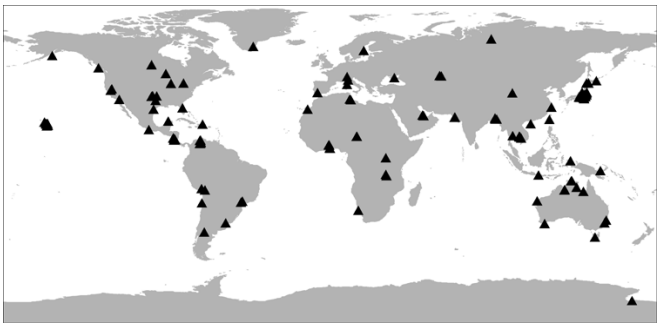

Fig. 5. Locations of the 163 ASTER scenes used for the emissivity-based validation.

applied to the surface radiance to obtain surface temperature and emissivity.

Fig. 4 shows the plot of the MMD of the retrieved emissivity versus the error on the retrieved temperature. As shown, the MMD and the surface temperature error do not have a one-to-one relationship, but they have roughly the following relationships:

$$\text{MMD} \simeq \begin{cases} 0.015 - 0.044 \times \delta T_S, & \text{if } \delta T_S < 0 \\ 0.015 + 0.015 \times \delta T_S, & \text{otherwise.} \end{cases} \quad (6)$$

The correlation coefficients are 0.68 and 0.79, respectively. These equations indicate that 0.05 on MMD is roughly corresponding to surface temperature errors of $-0.8\,^{\circ}\text{C}$ or $+2.3\,^{\circ}\text{C}$, although the deviation is large as shown in Fig. 4.

C. ASTER Data Used for Validation

For the emissivity-based validation, we collected 163 ASTER level-1B scenes [5] including water bodies, such as lakes, rivers, bays, and oceans, under clear sky conditions. Fig. 5 shows the locations of the 163 scenes. As shown, these scenes are almost globally distributed. Fig. 6 displays the histogram of the observation months of the 163 scenes, which indicates that nearly all seasons from March 2000 to March 2004 are included. In addition, the ASTER/TIR instrument can observe in nighttime as well as in daytime, although nighttime observations are less

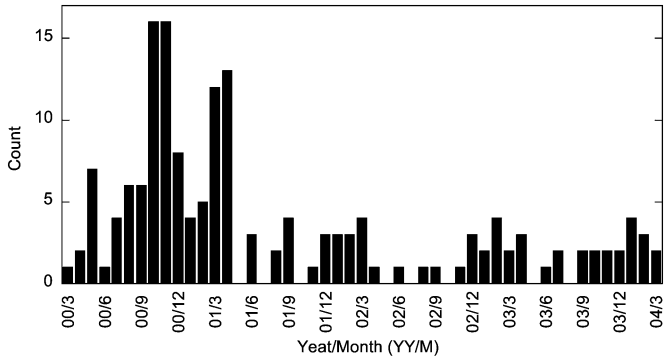

Fig. 6. Histogram of the observation months of the 163 ASTER scenes.

frequent than daytime observations. To check algorithm performance in nighttime scenes, we included 20 nighttime scenes in the 163 scenes.

D. Retrieval of Water Surface Emissivity

The target area selected from each scene is a square of 10×10 pixels (900×900 m^2) under a cloud-free condition. Fig. 7 shows the target areas for three scenes as examples. For each pixel in each target area, surface emissivity in each band was retrieved in the same way as Section V, and the MMD was calculated from the mean emissivity spectrum over the 100 pixels.

E. Results

Fig. 8 displays typical examples of water emissivity spectra retrieved with GDAS profiles, also showing the water emissivity spectrum derived from the spectral library. The spectrum of the case A is similar to the library spectrum, but the spectra of the other cases are different. In particular, the case C shows very different spectral behavior. From these examples, we can conclude that the standard atmospheric correction succeeded in the case A, but failed in the other cases, particularly in the case C. Obviously, the MMD of the retrieved emissivity increases with the atmospheric correction error, which indicates how the MMD of the retrieved emissivity is an effective index for assessing the quality of atmospheric correction performance.

Fig. 9 shows a comparison of PWV between GDAS and NRL for the 163 targets. The rms difference is 1.46 cm. As shown, NRL demonstrates no correlation in PWV with GDAS, and many points distribute around 2 cm. This is because the NRL model was created by averaging in zone and month. The results indicate that the NRL model will be less accurate than GDAS and will produce a larger error in higher humidy conditions.

Fig. 10 shows the plots of PWV versus MMD for GDAS and NRL with quadratic regression curves. The horizontal dashed line near each bottom indicates the MMD of the library emissivity ($= 0.0076$). The point for the worst case C in Fig. 8 is also shown in the left plot. In both GDAS and NRL, the variance of MMD increases quadratically with PWV, which indicates that the standard atmospheric correction will work well for a dry condition, but becomes progressively worse as the humidity increases. As shown, the NRL climatology produced larger errors than GDAS. The expected MMD error is 0.049 and 0.067 for GDAS and NRL, respectively, with a PWV of 3 cm (as shown

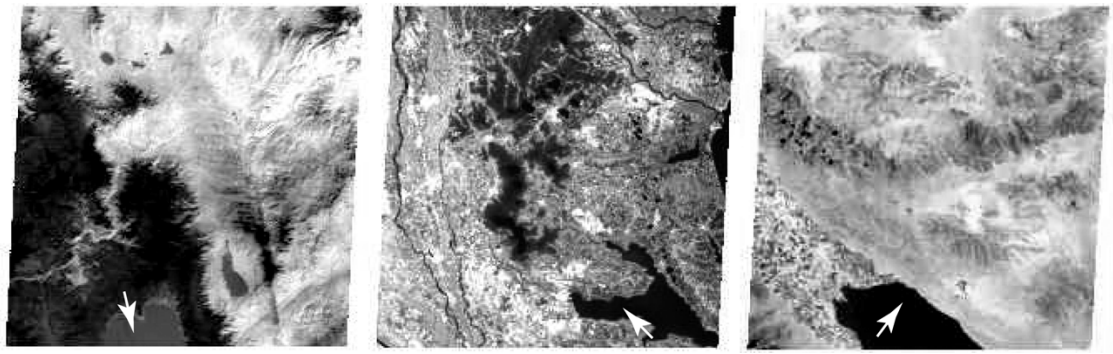

Fig. 7. Examples of the target areas selected (left) Lake Tahoe on March 12, 2000, (center) Lake Kasumigaura on May 16, 2000, and (right) Salton Sea on August 7, 2000.

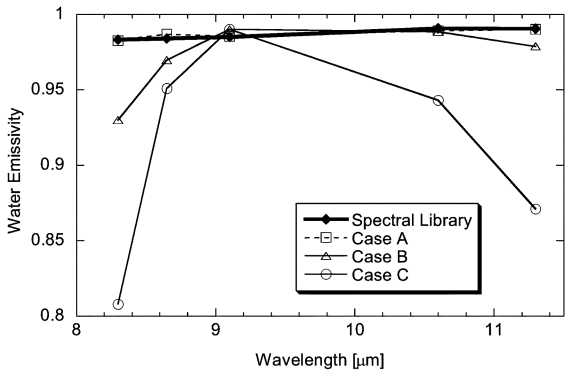

Fig. 8. Examples of water emissivity spectra retrieved with GDAS profiles. The water emissivity spectrum derived from the spectral library [36] is also shown. The case A is similar to the library spectrum, but the cases B and C are different because of atmospheric correction errors.

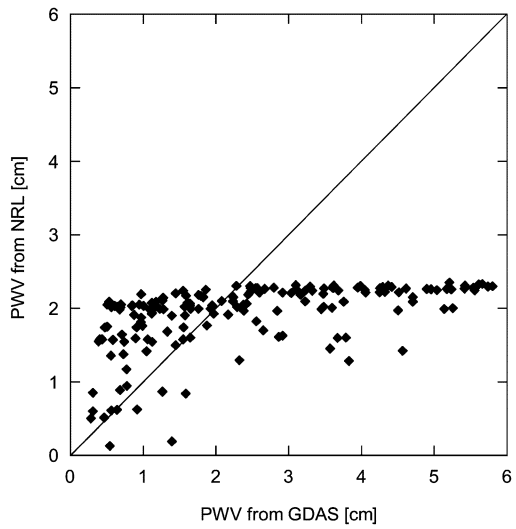

Fig. 9. Comparison of PWV between GDAS and NRL for the 163 targets. The correlation is low. The rms difference is 1.46 cm.

in Section VI-B, 0.05 on MMD is roughly corresponding to $-0.8\,^{\circ}$C or $+2.3\,^{\circ}$C on the retrieved surface temperature error).

Fig. 11 shows the plots of the surface temperature retrieved versus MMD for GDAS and NRL. In general, a high-temperature area will have a larger PWV due to more active evapotranspiration, except for arid regions. Thus, MMD is strongly correlated with surface temperature. The figure indicates that an atmospheric correction error will increase markedly if the surface temperature exceeds about 25 °C, particularly in the case of NRL, which are consistent well with the results from the *in situ* temperature-based validation, shown in Section V-E.

Incidentally, the algorithm performance was almost independent of the day/night difference in collection time.

VII. Conclusion

The standard atmospheric correction for ASTER/TIR has been validated by the temperature-based and the emissivity-based approaches.

In the temperature-based validation, *in situ* lake surface temperatures measured in 13 VC experiments were used. As the results, the mean bias was 0.8 and 1.8 K for GDAS and NRL, respectively. The NRL model performed much worse than GDAS for the four experiments at Salton Sea probably because the model is not suitable for the Salton Sea area which has typically higher surface temperature and humidity than other VC sites, but the NRL model exhibited similar performance to GDAS for the other experiments, although these experiments were conducted under lower humidy conditions by design.

In the emissivity-based validation, 163 globally distributed ASTER scenes were used, and the MMD of water emissivity retrieved was used as an index for assessing the performance of the algorithm. As the results, the algorithm error increased quadratically with PWV, and the expected MMD error was 0.049 and 0.067 for GDAS and NRL, respectively, with a PWV of 3 cm, where 0.05 on MMD is roughly corresponding to -0.8 or $+2.3$ K on the retrieved surface temperature error. In addition, the algorithm performance degraded markedly when the surface temperature exceeded about 25 °C, particularly in NRL.

Consequently, GDAS and NRL will work well for dry conditions, but the introduced error will increase with increasing atmospheric water content. GDAS will perform better than the NRL model in high humidity or high surface temperature conditions.

The water vapor scaling method has been proposed as an alternative atmospheric correction algorithm for ASTER/TIR [39]. This method is based on the standard algorithm but will give more accurate results in most cases. A validation study on this algorithm will be described in another paper [40].

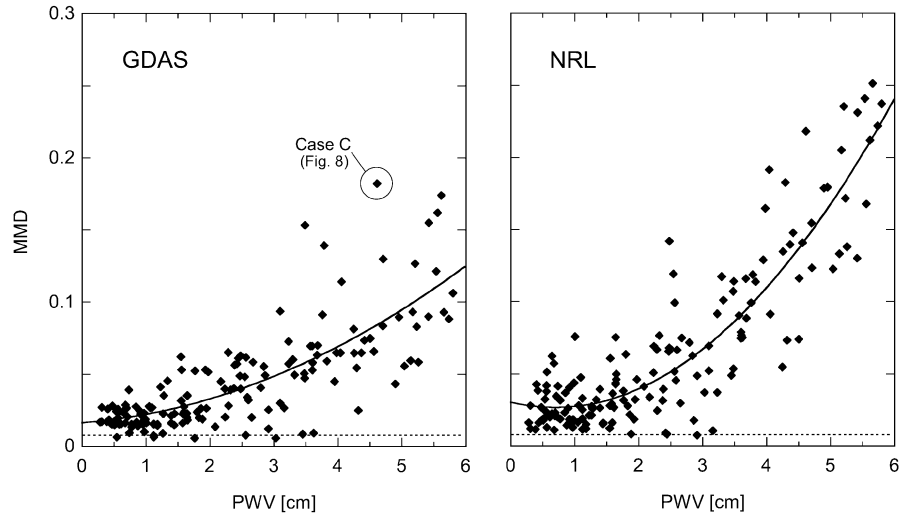

Fig. 10. Plots of PWV versus MMD for GDAS and NRL with quadratic regression curves. The horizontal dashed line near each bottom indicates the MMD of the library emissivity ($= 0.0076$). The point for the worst case C in Fig. 8 is also shown in the left plot. The PWV derived from GDAS is used for the horizontal axis. The variance of MMD increases quadratically with PWV. GDAS shows better results than NRL.

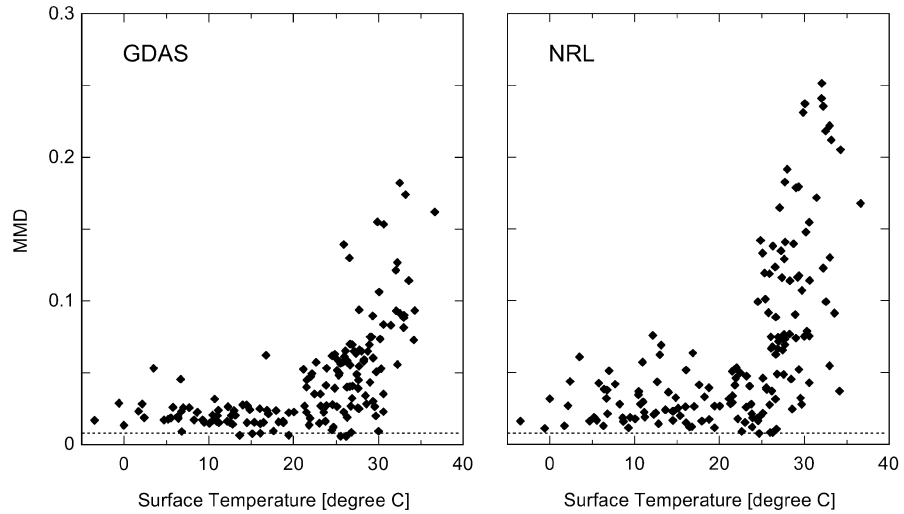

Fig. 11. Plots of the surface temperature retrieved versus MMD for GDAS and NRL. An atmospheric correction error will increase markedly if the surface temperature exceeds about 25 °C, particularly in the case of NRL.

ACKNOWLEDGMENT

The authors would like to thank Earth Remote Sensing Data Analysis Center, Tokyo, for supplying original ASTER data and for supporting the vicarious calibration experiments, and the U.S./Japan ASTER Science Team Members for useful discussions.

REFERENCES

[1] Y. Yamaguchi, A. B. Kahle, H. Tsu, T. Kawakami, and M. Pniel, "Overview of Advanced Spaceborne Thermal Emission and Reflectance radiometer (ASTER)," *IEEE Trans. Geosci. Remote Sens.*, vol. 36, no. 4, pp. 1062–1071, Jul. 1998.

[2] T. J. Schmugge, A. French, J. Ritchie, A. Rango, and H. Pelgrum, "Temperature and emissivity separation from multispectral thermal infrared observations," *Remote Sens. Environ.*, vol. 79, pp. 189–198, 2002.

[3] F. Jacob, F. Petitcolin, T. Schmugge, E. Vermote, K. Ogawa, and A. French, "Comparison of land surface emissivity and radiometric temperature from MODIS and ASTER sensors," *Remote Sens. Environ.*, vol. 83, pp. 1–18, 2004.

[4] H. Tonooka and F. Palluconi, "Verification of the ASTER/TIR atmospheric correction algorithm based on water surface emissivity retrieved," *Proc. SPIE*, vol. 4486, pp. 51–58, 2001.

[5] H. Fujisada, "ASTER level-1 data processing algorithm," *IEEE Trans. Geosci. Remote Sens.*, vol. 36, no. 4, pp. 1101–1112, Jul. 1998.

[6] H. Tonooka, F. Sakuma, M. Kudoh, and K. Iwafune, "ASTER/TIR onboard calibration status and user-based recalibration," *Proc. SPIE*, vol. 5234, pp. 191–201, 2003.

[7] H. Tonooka, F. Palluconi, S. Hook, and T. Matsunaga, "Vicarious calibration of ASTER thermal infrared bands," *IEEE Trans. Geosci. Remote Sens.*, vol. 43, no. 12, pp. 2733–2746, Dec. 2005.

[8] Z. Wan and Z.-L. Li, "Physics-based algorithm for retrieving land-surface emissivity and temperature from EOS/MODIS data," *IEEE Trans. Geosci. Remote Sens.*, vol. 35, no. 4, pp. 980–996, Jul. 1997.

[9] F. Becker and Z.-L. Li, "Temperature-independent spectral indexes in thermal infrared bands," *Remote Sens. Environ.*, vol. 32, pp. 17–33, 1990.

[10] F. X. Kneizys, L. W. Abreu, G. P. Anderson, J. H. Chetwynd, E. P. Shettle, A. Berk, L. S. Bernstein, D. C. Robertson, P. Acharya, L. S. Rothman, J. E. A. Selby, W. O. Gallery, and S. A. Clough, "The MODTRAN 2/3 Report and LOWTRAN 7 Model," Phillips Lab., Hanscom AFB, MA, F19628-91-C-0132, 1996.

[11] J. C. Price, "Land surface temperature measurements from the split window channels of the NOAA 7 Advanced Very High Resolution Radiometer," *J. Geophys. Res.*, vol. 89, no. D5, pp. 7231–7237, 1984.
[12] S. J. Hook, A. R. Gabell, A. A. Green, and P. S. Kealy, "A comparison of techniques for extracting emissivity information from thermal infrared data for geologic studies," *Remote Sens. Environ.*, vol. 42, no. 2, pp. 123–136, 1992.
[13] C. Ottlé and D. Vidal-Madjar, "Estimation of land surface temperature with NOAA9 data," *Remote Sens. Environ.*, vol. 40, pp. 27–41, 1992.
[14] C. Ottlé and M. Stoll, "Effect of atmospheric absorption and surface emissivity on the determination of land surface temperature from infrared satellite data," *Int. J. Remote Sens.*, vol. 14, no. 10, pp. 2025–2037, 1993.
[15] F. Jacob, X. F. Gu, J.-F. Hanocq, and F. Baret, "Atmospheric corrections of single broad-band channel and multidirectional airborne thermal infrared data. Application to the ReSeDa experiment," *Int. J. Remote Sens.*, vol. 24, pp. 3269–3290, 2003.
[16] V. J. Realmuto, "Separating the effects of temperature and emissivity: Emissivity spectrum normalization," presented at the *2nd TIMS Workshop*, Pasadena, CA, 1990.
[17] L. M. McMillin, "Estimation of sea surface temperatures from two infrared window measurements with different absorption," *J. Geophys. Res.*, vol. 80, no. 36, pp. 5113–5117, 1975.
[18] C. Prabhakara, G. Dalu, and V. G. Kunde, "Estimation of sea surface temperature from remote sensing in the 11- to 13-μm window region," *J. Geophys. Res.*, vol. 79, no. 33, pp. 5039–5044, 1974.
[19] P. Y. Deschamps and T. Phulpin, "Atmospheric correction of infrared measurements of sea surface temperature using channels at 3.7, 11 and 12 μm," *Bound. Layer Method*, vol. 18, pp. 131–143, 1980.
[20] K. B. Kidwell, *NOAA Polar Orbiter Data Users Guide*. Washington, DC: NOAA, 1995.
[21] F. Becker, "The impact of spectral emissivity on the measurement of land surface temperature from a satellite," *Int. J. Remote Sens.*, vol. 8, no. 10, pp. 1509–1522, 1987.
[22] F. Becker and Z.-L. Li, "Toward a local split window method over land surfaces," *Int. J. Remote Sens.*, vol. 11, no. 3, pp. 369–393, 1990.
[23] J. A. Sobrino, C. Coll, and V. Caselles, "Atmospheric correction for land surface temperature using NOAA-11AVHRR channels 4 and 5," *Remote Sens. Environ.*, vol. 38, pp. 19–34, 1991.
[24] Y. H. Kerr, J. P. Lagouarde, and J. Imbernon, "Accurate land surface temperature retrieval from AVHRR data with use of an improved split window algorithm," *Remote Sens. Environ.*, vol. 41, pp. 197–209, 1992.
[25] J. A. Sobrino, Z. L. Li, M. P. Stoll, and F. Becker, "Improvements in the split-window technique for land surface temperature determination," *IEEE Trans. Geosci. Remote Sens.*, vol. 32, no. 2, pp. 243–253, Mar. 1994.
[26] Z. Wan and J. Dozier, "A generalized split-window algorithm for retrieving land-surface temperature from space," *IEEE Trans. Geosci. Remote Sens.*, vol. 34, no. 4, pp. 892–905, Jul. 1996.
[27] F. Palluconi, G. Hoover, R. Alley, M. J. Nilsen, and T. Thompson, "An atmospheric correction method for ASTER thermal radiometry over land, ASTER. Algorithm Theoretical Basis Document (ATBD), Revision 3," Jet Propulsion Lab., Pasadena, CA, 1999.
[28] E. Kalnay, M. Kanamitsu, and W. E. Baker, "Global numerical weather prediction at the national meteorological center," *Bull. Amer. Meteorol. Soc.*, vol. 71, no. 10, pp. 1410–1428, 1990.
[29] M. E. Summers and W. Sawchuck, "Zonally averaged trace constituent climatology," Naval Res. Lab., Washington, DC, NRL Tech. Pub. RL/MR/7641-93-7416, 1993.
[30] W. P. Menzel and L. E. Gumley, "MODIS atmospheric profile retrieval. Algorithm Theoretical Basis Document, Version 4," Univ. Wisconsin, Madison, WI, 1998.
[31] R. D. McPeters, P. K. Bhartia, A. J. Krueger, J. R. Jaross, O. Torres, L. Moy, G. Labow, W. Byerly, S. L. Taylor, T. Swissler, and R. P. Cebula, "Earth probe Total Ozone Mapping Spectrometer (TOMS) data products user's guide," NASA, Greenbelt, MD, NASA Tech. Pub. 1998-206895, 1998.
[32] USGS. (2004) GTOPO30—Global Topographic Data. U.S. Geol. Surv., Sioux Falls, SD. [Online]. Available: http://edcdaac.usgs.gov/gtopo30/gtopo30.asp.
[33] P. Slater, S. F. Biggar, K. Thome, D. I. Gellman, and P. R. Spyak, "Vicarious radiometric calibrations of EOS sensors," *J. Atmos. Oceanic Technol.*, vol. 13, pp. 349–359, 1996.
[34] K. Thome, K. Arai, S. Hook, H. Kieffer, H. Lang, T. Matsunaga, A. Ono, F. Palluconi, H. Sakuma, P. Slater, T. Takashima, H. Tonooka, S. Tsuchida, R. Welch, and E. Zalewski, "ASTER preflight and inflight calibration and the validation of level 2 products," *IEEE Trans. Geosci. Remote Sens.*, vol. 36, no. 5, pp. 1161–1172, Sep. 1998.
[35] F. D. Palluconi, H. Tonooka, A. Abtahi, R. E. Alley, T. Thompson, G. Hoover, and S. Zadourian, "EOS ASTER midinfrared band vicarious calibration," *Proc. SPIE*, vol. 4540, pp. 255–259, 2002.
[36] S. J. Hook. (1999) The ASTER Spectral Library. [Online]. Available: http://speclib.jpl.nasa.gov.
[37] J. W. Salisbury and D. M. D'Aria, "Emissivity of terrestrial materials in the 8–14 μm atmospheric window," *Remote Sens. Environ.*, vol. 42, pp. 83–106, 1992.
[38] K. Masuda, T. Takashima, and Y. Takayama, "Emissivity of pure and sea waters for the model sea surface in the infrared window regions," *Remote Sens. Environ.*, vol. 24, no. 2, pp. 313–329, 1988.
[39] H. Tonooka, "An atmospheric correction algorithm for thermal infrared multispectral data over land—A water vapor scaling method," *IEEE Trans. Geosci. Remote Sens.*, vol. 39, no. 3, pp. 682–692, Mar. 2001.
[40] ——, "Accurate atmospheric correction of ASTER thermal infrared imagery using the WVS method," *IEEE Trans. Geosci. Remote Sens.*, vol. 43, no. 12, pp. 2778–2792, Dec. 2005.

Hideyuki Tonooka (M'04) received the B.Eng., M.Eng., and D.Eng. degrees from the University of Tokyo, Tokyo, Japan, in 1992, 1994, and 2000, respectively.

Since 1994, he has been a member of the faculty of Ibaraki University, Ibaraki, Japan. His current post at the university is Associate Professor in the Center for Information Technology. He is a member of the Project Science Team for the Advanced Spaceborne Thermal Emission and Reflection radiometer (ASTER), part of the National Aeronautics and Space Administration's Earth Observing System, and he is also a member of the Thermal Infrared Science Team for the Greenhouse gas Observing SATellite (GOSAT) under development by the Japan Aerospace Exploration Agency and the Ministry of the Environment of Japan. His main research activities are in thermal infrared remote sensing and data fusion techniques.

Frank D. Palluconi is a Member of the Jet Propulsion Laboratory, Pasadena, CA, and has an interest in thermal measurement instrumentation, atmospheric correction, and their application to the understanding of planetary surfaces and surface processes. He is a NASA Earth Observing System ASTER Team Member, a Landsat-7 Calibration Team Member, and a Scientist working on the Mars Science Laboratory 2009 Rover Mission.